Geoderma 383 (2021) 114780

Contents lists available at ScienceDirect

Geoderma

journal homepage: www.elsevier.com/locate/geoderma

Impact of climate, soil properties and grassland cover on soil water repellency

Renáta Sándor [a,*], Massimo Iovino [b], Lubomir Lichner [c], Vincenzo Alagna [b,d], Daniel Forster [e], Mariecia Fraser [e], Jozef Kollár [f], Peter Šurda [c], Viliam Nagy [c], Anita Szabó [g], Nándor Fodor [a]

[a] Agricultural Institute, Centre for Agricultural Research, Brunszvik u. 2, 2462 Martonvásár, Hungary
[b] Department of Agricultural, Food and Forest Sciences, University of Palermo, Viale delle Scienze, Ed. 4 Ingr. E, 90128 Palermo, Italy
[c] Institute of Hydrology, Slovak Academy of Sciences, Dúbravská cesta 9, 841 04 Bratislava, Slovak Republic
[d] Department of Agricultural and Food Sciences (DISTAL), Alma Mater Studiorum, University of Bologna, Viale Giuseppe Fanin, 50, 40127 Bologna, Italy
[e] Pwllpeiran Upland Research Centre, Aberystwyth University, Cwmystwyth, Aberystwyth, Ceredigion SY23 4AD, United Kingdom
[f] Institute of Landscape Ecology, Slovak Academy of Sciences, Štefánikova 3, 81499 Bratislava, Slovak Republic
[g] Institute for Soil Sciences and Agricultural Chemistry, Centre for Agricultural Research, Herman Otto út 15, 1022 Budapest, Hungary

ARTICLE INFO

Handling Editor: Morgan Cristine L.S.

Keywords:
Soil properties
Soil water repellency
Grass
Length of dry periods
Climate factors

ABSTRACT

Numerous soil water repellency (SWR) studies have investigated the possible causes of this temporal phenomenon, yet there remains a lack of knowledge on the order of importance of the main driving forces of SWR in the context of changing environmental conditions under grassland ecosystems. To study the separate and combined effects of soil texture, climate, and grassland cover type on inducing or altering SWR, four sites from different climatic and soil regions were selected: Ciavolo (CI, IT), Csólyospálos (CSP, HU), Pwllpeiran (PW, UK), Sekule (SE, SK). The investigated parameters were the extent (determined by repellency indices *RI, RI_c* and *RI_m*) and persistence (determined by water drop penetration time (WDPT) and water repellency cessation time, WRCT) of SWR, as well as field water (S_w) and ethanol (S_e) sorptivity, water sorptivity of hydrophobic soil state (S_{wh}) water sorptivity of nearly wettable soil state (S_{ww}) and field hydraulic conductivity (K). Our findings showed an area of land has a greater likelihood of being water repellent if it has a sandy soil texture and/or a high frequency of prolonged drought events. Water infiltration was positively correlated with all the sorptivities ($r = 0.32$–0.88), but was mostly negatively correlated with *RI* ($r = -0.54$ at CI), WDPT ($r = -0.47$ at CI) and WRCT ($r = -0.58$ at CI). The importance of natural and synanthropized vegetation covers with regards to SWR was not coherent; moving to regions having coarser texture or moving to drier climatic zones led to higher risk of SWR conditions. Climate change has been predicted to lead to more frequent extreme weather events and prolonged dry periods across Europe, which will most likely increase the extent of SWR-affected areas and increase the role of SWR in water management of grassland ecosystems. Therefore, there is a need to determine SWR risk zones to prevent decreases in soil moisture content, soil fertility, carbon and nitrogen sink potentials, as well as biomass production of the related agro-ecosystems.

1. Introduction

More than one fifth (20.7%) of EU-28′s area is covered by temperate grasslands (EUROSTAT, 2015). These grasslands are characterized by considerable plant diversity depending on environmental conditions, management practices (grazing, mowing) and land use intensity (Fischer et al., 2015). Vegetation can have beneficial effects on surface hydrologic properties, including increasing infiltration capacity and erosion control (Moreno-de Las Heras et al., 2009). Mechanisms associated with these effects include soil organic matter accumulation and soil aggregation, the prevention of soil crusting, development of sub-surface channels in association with plant rooting (Alaoui et al., 2011; Beven and Germann, 2013; Clark and Zipper, 2016). Besides the listed beneficial effects of vegetation cover on hydrologic properties, the hydrophobic compounds released from roots (Robinson et al., 2010) may significantly change soil–water interactions at the soil surface with potentially negative effects on soil hydrological processes (e.g., Doerr et al., 2000).

* Corresponding author.
E-mail address: sandor.renata@atk.hu (R. Sándor).

https://doi.org/10.1016/j.geoderma.2020.114780
Received 20 May 2020; Received in revised form 8 October 2020; Accepted 11 October 2020
Available online 1 November 2020

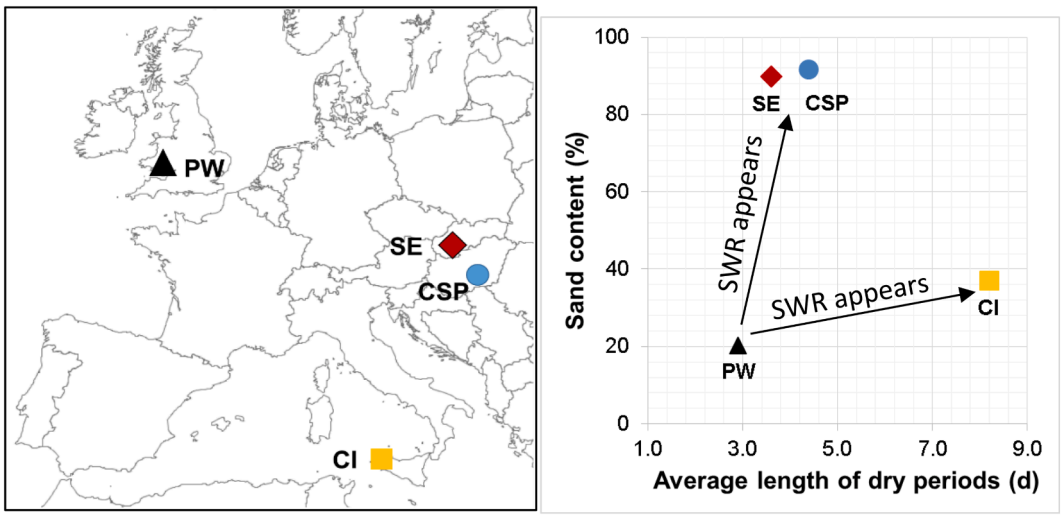

Fig. 1. Geographical location (left) and classification (right) of grassland sites with respect to sand content and average length of dry periods. CI: Ciavolo (IT); CSP: Csólyospálos (HU); PW: Pwllpeiran (UK); SE Sekule (SK).

Soil water repellency (SWR) is a surface property of soil caused by hydrophobic compounds (SWR markers, Mao et al., 2016) which can develop in soils of varying textural composition from clay (Dekker and Ritsema, 1996) to sand (Lichner et al., 2012). Previous studies have shown that soil pH (Diehl et al., 2010), quality of organic matter (e.g. the amount of wax) (Bisdom et al., 1993; Doerr et al., 2000; Lichner et al., 2012), abundancy of soil microbiota (Hallett and Young, 1999, Rillig et al., 2010), particle and aggregate coatings, ionic soil solution composition (Doerr, 1998; Diehl, 2013), actual soil structure (Bisdom et al., 1993), soil temperature (Doerr, 1998), and soil water content may redound the development or the temporal occurrence of SWR causing negative changes in soil moisture regime.

SWR has positive effects on the stability of soil aggregates (Fér et al., 2016; Goebel et al., 2005) and may reduce losses of soil water by evaporation (Bachmann et al., 2001). Rye and Smettem (2017) also concluded that water repellent surface layers can bring about significant reductions in net evaporative moisture loss, in which case the phenomenon of SWR has positive impacts on water budgets, the grassland ecosystem and its services. On the other hand, SWR can lead to irregular moisture patterns, e.g. preferential flow (Täumer et al., 2006), or to a diminished infiltration enhancing overland flow, and consequently increases the risk of surface runoff, soil erosion and surface waters pollution (Diehl, 2013; Doerr et al., 2000; Orfánus et al., 2014, 2016). Due to reduced soil-water redistribution resulting in poor germination and plant growth, reduced agricultural productivity can be found in water repellent soils (Roper, 2005; Ward et al., 2015). Furthermore, rewetting of water-repellent soils could have an enhanced effect on pathogen (such as *Rhodococcus erythropolis*) release and transport (Sepehrnia et al., 2019). Additional studies showed that SWR can be significantly decreased by adding lime, kaolinite clay, or wax degrading bacteria to the soil (Lichner et al., 2002; McKissock et al., 2000; Roper, 2005; 2006).

Changing global environmental conditions (e.g. temperature and precipitation) also have a significant effect on SWR and plant community structure (Kneitel, 2010), and thus indirectly affect worldwide food production and security. Temperature change is among the key drivers of our future climate, and global mean land surface air temperatures over terrestrial areas have already increased by 1.53 °C from 1850 to 1900 to 2006–2015 (IPCC, 2019). More frequent extreme arid years are predicted for the future, with longer dry spells, drought periods (Meehl et al., 2007) and heatwaves (Fischer and Schär, 2010). As the changes in temperature and precipitation will not be uniform, the outcomes will vary between different climate zones. In dry summers, available soil water content (SWC) for vegetation is also reduced by the phenomenon of SWR, which shows significant seasonal variability (Müller et al. 2014) and spatial heterogeneity (Sándor et al., 2015). SWR is generally found to be the most extreme when soils are dry, declining and eventually disappearing as soils become wet (de Jonge et al., 1999; Dekker and Ritsema, 1994; Fér et al., 2016; Lichner et al., 2013). This is the main reason why heavy rainfalls after longer dry periods may result in considerable surface runoff (Imeson et al., 1992) and soil erosion (Doerr and Moody 2004). Müller et al. (2018) identified the SWR as a factor leading to runoff and phosphorus losses, where about 20% of the applied 45 kg P ha^{-1} fertilizer was lost to runoff. Thus, the predicted increase in annual mean global temperature and heatwave frequency is expected to influence SWR and the related soil water balance processes in the future (Goebel et al., 2011). The phenomena of SWR is not only present in arid and semiarid regions; e.g. Lozano-Baez et al. (2020) detected it in the Atlantic Forest region of Brazil. For this reason, it is essential to clarify those criteria which could turn a balanced or carbon sequestrating grassland ecosystem into a carbon releasing environment owing to enhanced effects of SWR related to climate change.

The objectives of this study were to demonstrate the effect of different factors on SWR for sites with different soil, climatic and vegetation characteristics by: i) analysing the effect of the two most important factors (soil texture and climate), ii) describing the differences in SWR as a consequence of different grassland cover across the investigated soil types and climatic regions, iii) identifying the circumstances with potentially high and low chance of water repellency in order to support the reduction of the negative effects of SWR on the ecosystem.

2. Material and methods

To determine the effect of different climate and soil properties on the severity of SWR, four locations were selected across Europe: in Italy, Hungary, Slovakia and the UK (Fig. 1). This approach to site selection provided opportunities to test different combinations of climate (short *vs* long dry periods) and soil texture (coarse *vs* fine texture). The two Eastern-European sites (cf. Fig. 1) were characterised in the greatest detail, particularly with regards to vegetation cover. SWR experiments were carried out in September of 2016 at Pwllpeiran and Ciavolo, and in June and September of 2017 at Sekule and Csólyospálos sites, respectively. All cases the measurements were taken after at least five consecutive dry days. Daily meteorological datasets were available from 1980 to 2017 for all the sites. Each experimental area was investigated

Table 1
Climatic circumstances (±their standard deviations) of the experimental sites at Ciavolo (CI, Italy), Csólyospálos (CSP, Hungary), Pwllpeiran (PW, UK) and Sekule (SE, Slovakia) between 1980 and 2017. Summer temperatures were measured between 1st of June and 31st of August.

Climatic characteristics	Site (Abbreviation)			
	Ciavolo (CI)	**Csólyospálos** (CSP)	**Pwllpeiran** (PW)	**Sekule** (SE)
Köppen-Geiger climate classification	Csa	Cfa, Dfb	Cfb	Cfb
Average annual temperature (°C)	~17.9 ± 0.7	~14.0 ± 0.8	~ 9.5 ± 0.7	~ 12.2 ± 0.8
Average summer temperature (°C)	~24.4 ± 1.0	~24.5 ± 1.1	~14.6 ± 1.0	~22.4 ± 1.2
Average of maximal summer temperature (°C)	~37.4 ± 2.6	~36.2 ± 1.6	~27.7 ± 3.0	~34.2 ± 2.6
Average annual precipitation (mm)	~587 ± 157	~520 ± 195	~1313 ± 488	~542 ± 167
de Martonne-Gottmann Aridity index (category)	~10.6 ± 2.9 (arid)	~14.4 ± 6.5 (semi-arid)	~44.8 ± 19.2 (humid)	~16.2 ± 6.2 (semi-arid)
Rainfall seasonality index	~ –0.46 ± 0.17	~0.18 ± 0.16	~ –0.08 ± 0.13	~ 0.21 ± 0.13
Maximum length of dry period	99 ± 21	50 ± 7.7	31 ± 6.1	37 ± 6.1
Mean length of dry periods between 1st Apr and 31st Oct	8.2 ± 2.3	4.7 ± 0.7	2.9 ± 0.8	3.6 ± 0.8

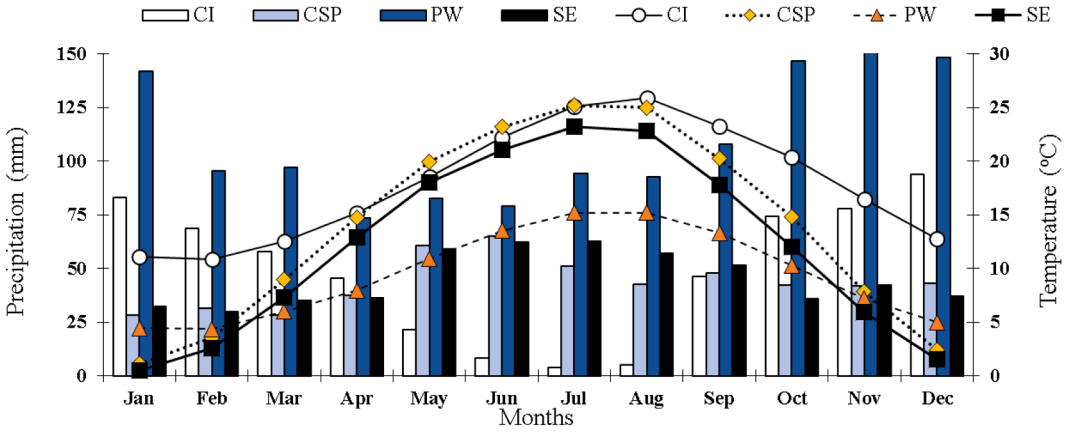

Fig. 2. Monthly mean temperature (°C) and precipitation (mm) at CI: Ciavolo (IT); CSP: Csólyospálos (HU); SE Sekule (SK); PW: Pwllpeiran (UK) sites between 1980 and 2017.

Table 2
Physical and chemical properties (±their standard deviations) of the top (0–5 cm) soils taken from the experimental sites/sub-sites CI (Ciavolo, Italy), CSP17, CSP44 (Csólyospálos, Hungary), PW (Pwllpeiran, Wales, UK), and SeN, SeS (Sekule, Slovakia). (OC – organic carbon content).

Site	Sand (%)	Silt (%)	Clay (%)	$CaCO_3$ (%)	OC (%)	pH (H_2O)	Bulk density (g cm^{-3})
CI	36.92 ± 0.23	34.55 ± 0.24	28.53 ± 0.01	3.80 ± 0.15	2.73 ± 0.28	7.77 ± 0.19	1.19
CSP17	94.93 ± 0.30	3.15 ± 0.28	1.92 ± 0.03	2.80 ± 0.31	0.64 ± 0.12	8.13 ± 0.07	1.41
CSP44	88.14 ± 0.42	9.53 ± 0.35	2.34 ± 0.04	2.87 ± 0.25	2.09 ± 0.03	7.81 ± 0.13	1.40
PW	20.19 ± 1.44	58.36 ± 1.59	21.45 ± 0.93	0	7.77 ± 1.45	5.67 ± 0.21	1.21
SeN	88.45 ± 0.40	7.35 ± 0.29	4.20 ± 0.10	0	5.39 ± 0.07	5.20 ± 0.01	1.42
SeS	91.30 ± 0.35	2.80 ± 0.10	5.90 ± 0.22	0	9.90 ± 0.12	5.14 ± 0.03	1.41

on a pedon scale, which is generally considered to be 'homogenous'. Approximately 0.5–1 cm thick soil layer was removed before the measurements to reduce the influence of, e.g., aggregates compacted by rain or vegetation residues on water repellency (Rodríguez-Alleres and Benito, 2011). An area of around 1 m^2 area was divided into 20 cm × 20 cm cells, where SWC, water drop penetration time (WDPT), field unsaturated hydraulic conductivity (K), water sorptivity (S_w, S_{ww}, S_{wh}), repellency indexes (RI, RI_c, RI_m) and water repellency cessation time (WRCT) were measured in 5–25 replications, while ethanol sorptivity (S_e) was measured in 5–11 replications. Sand, silt, clay, $CaCO_3$, and organic carbon contents were determined in the laboratory using sieved (2-mm-mesh sieve), mixed, and air-dried (at 30 °C) samples collected from the topsoil (0–5 cm) of the experimental sites in 3 to 10 repetitions. The initial SWC was measured from each cells of the field measurement quadrat using a HH2 Soil Moisture Meter combined with WET-2 sensor (Delta-T Devices, Cambridge, UK). Potential WDPT ($WDPT_P$) of the PW soil was measured in laboratory on dried samples (SWC = ~0.00 m^3 m^{-3}) in five repetitions, because the SWC value was too high there during the field measurements.

2.1. Study sites

The first experimental site is located in Ciavolo on the island of Sicily, Italy (37°45′40.6″ N, 12°34′09.0″ E), in a pine forest glade (site CI) vegetated with spontaneous annual grasses. According to the Köppen-Geiger climate classification, the region has a Mediterranean temperate climate with a dry and hot summer (Csa) (Kottek et al., 2006) and winter domination of precipitation (rainfall seasonality index <

Table 3
The major vegetation constituents recorded in quadrats of the experimental sites/sub-sites CI (Ciavolo, Italy), CSP17, CSP44 (Csólyospálos, Hungary), PW (Pwllpeiran, Wales, UK), and SeN, SeS (Sekule, Slovakia) before the measurements.

Site	Year	Floristic province	Species composition
CI	2016	Mediterranean	*Avena fatua, Galactites elegans, Hypochaeris achyrophorus, Oxalis pes-caprae, Vulpia ciliata*
CSP17	2017	*Pannonicum, Praematricum*	*Elymus repens, Bromus tectorum, B. sterilis, Polygonum aviculare, Poa angustifolia, Silene latifolia* subsp. *alba, Hordeum murinum, Lamium purpureum*
CSP44			*Festuca vaginata, F. pseudovina, F. rupicola, Poa angustifolia, Echium vulgare, Silene latifolia* subsp. *alba, Erodium cicutarium*
PW	2016	Calcifugous grasslands and montane communities	*Lolium perenne, Agrostis capillaris, Trifolium repens, Ranunculus repens, Festuca ovina, Holcus lanatus, Cirsium arvense, Anthoxanthum odoratum, Cynosurus cristatus, Leontodon autumnalis, Dactylis glomerata, Ranunculus acris, Rumex acetosa, Taraxacum officinale* agg.
SeN	2017	*Pannonicum*	*Festuca rupicola, F. vaginata, Carex supina, Potentilla arenaria, Rumex acetosella, Armeria maritima, Eryngium campestre, Euphorbia cyparissias, Veronica dillenii, Teucrium chamaedrys*
SeS			*Poa angustifolia, Agrostis capillaris, Cynodon dactylon, Eryngium campestre, Festuca rupicola, Calamagrostis epigejos, Carex hirta, Convolvulus arvense, Achillea millefolium* agg., *Equisetum ramosissimum, Plantago lanceolata, Euphorbia cyparissias, Senecio jacobea*

–0.13, Table 1) with arid climate (Table 1). The multi-year monthly average temperature and precipitation values also show summer drought events (Fig. 2). Elevation at the experimental site is 105 m a.s.l. and the surface slope is low (4.4%). The soil is a Calcaric Chromic Endoleptic Cambisol (WRB, 2014) with a depth of 0.40–0.60 m and the parent material is calcareous sandstone. According to Soil Survey Division Staff (1993) the soil texture is clay loam (Table 2) and covered by Mediterranean species listed in Table 3.

The second experimental site (with two grassland sub-sites) is located in Csólyospálos, Hungary (46°25′05′′ N, 19°50′28′′ E). According to the Köppen-Geiger climate classification, the region has a temperate climate without a dry season, hot summer (Cfa) (Kottek et al., 2006), however some years show the characteristic of humid continental climate (Dfb). Table 1 shows the most important climate details and Fig. 2 demonstrates the monthly distribution of precipitation and temperature over years. The average annual rainfall is ~ 520 ± 195 mm with ~ 60% dominance of summer precipitation, while the rest 40% of the investigated period characterised by uniform distribution. Elevation at the experimental site is 102.6 m a.s.l. Sub-site CSP17, abandoned for 17 years, was covered by strongly synanthropized vegetation – poor grassland dominated by perennial weedy grass and annual grasses (listed in Table 3). Sub-site CSP44, abandoned for 44 years, was covered by successionally more advanced grassland dominated by perennial grasses with an admixture of mostly weedy herbs (listed in Table 3). The soil is an Arenosol (WRB, 2014) and has sandy texture (Soil Survey Division Staff, 1993) (Table 2) the parent material is aeolian calcareous non-structural sand.

The third experimental site is located at Pwllpeiran, mid Wales, UK (52°21′53′′ N, 03°49′39′′ W), on an upland pasture with a long agricultural history, vegetated mostly with *Lolium perenne* and other species listed in Table. 3 (site PW). According to the Köppen-Geiger climate classification, the region has a moderate marine climate (type Cfb; Kottek et al., 2006) with quite cold summers, ~14.6 ± 1.0 °C, and precipitation all year round (Table 1, Fig. 2). Elevation at experimental site is 310 m a.s.l. The soil is Typical Brown Podzolic soil (WRB, 2014) and has a silt loam texture (Soil Survey Division Staff, 1993) (Table 2), with a bedrock depth of between 0.6 and 1 m.

The fourth experimental site (with two grassland sub-sites) is located at Sekule (48°37′10′′ N, 17°00′10′′ E) in the Borská nížina lowland (southwest Slovakia). According to the Köppen-Geiger climate classification, the region has a temperate climate without dry season, warm summer (Cfb) (Kottek et al., 2006). Mean annual precipitation is ~542 mm, which is summer-dominant (Table 1) as is shown in Fig. 2. Elevation is 158 m a.s.l. and surface slope is negligible. Sub-site SeN with natural vegetation undisturbed by human activities was dominated by the grasses (Table 3). Of cryptogams, the mosses *Bryum capillare*, *Hypnum cupressiforme*, *Brachythecium albicans*, and the lichen *C. furcata* were recorded. Sub-site SeS with synanthropized vegetation formed by secondary succession triggered by some anthropogenous disruptions was covered by species listed in Table 3. The soil is an Arenosol (WRB, 2014) and has sandy texture (Soil Survey Division Staff, 1993) and the parent material is aeolian siliceous sand.

2.2. Field methods

All the field measurements were carried out on the surface of the studied soils after at least five consecutive rainless days. Field water and ethanol infiltration measurements were performed with a minidisk infiltrometer (MDI, Decagon Devices, 2012) under a pressure head value of $h_0 = -2$ cm. A pressure head of –2 cm was selected, because tension infiltration experiments are preferred to ponded ones to exclude the contribution of macropores that may overwhelm soil hydrophobicity (Nyman et al., 2010). The sorptivity, S (m s$^{-1/2}$), was estimated from the cumulative infiltration, I (m) (Clothier et al., 2000):

$$S(h_0) = I / t^{0.5} \quad (1)$$

Eq. (1) was used to calculate both the water (S_w (m s$^{-1/2}$)) and ethanol sorptivity (S_e (m s$^{-1/2}$)) from the cumulative infiltration *vs.* square root of the time relationships taken from the minidisk infiltrometer measurements (Alagna et al., 2018).

Zhang (1997) proposed using the first two terms of the Philip infiltration equation to estimate the soil hydraulic conductivity $K(h_0)$ (m s^{-1}):

$$K(h_0) = C_2/A \quad (2)$$

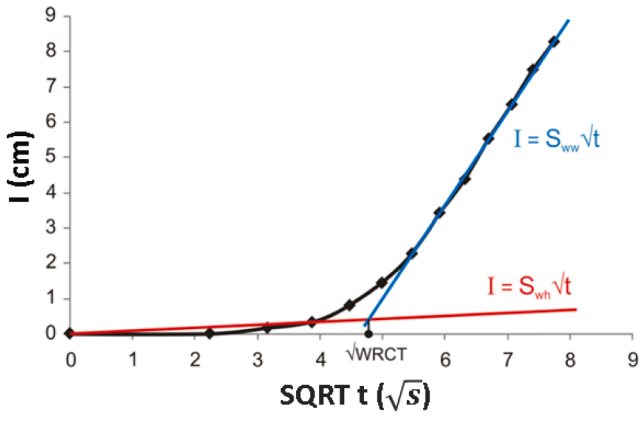

Fig. 3. The hockey-stick-like relationship of the cumulative infiltration of water (I) against the square root of time (SQRT t) for sandy soil from the Csólyospálos site. The water sorptivity (S_{wh}) for water-repellent state of soil and the water sorptivity (S_{ww}) for nearly wettable state of soil were estimated, respectively, from the less steep and steeper parts of hockey-stick-like relationship. The WRCT was estimated from the point of intersection of two straight lines, representing the I = f(SQRT t) relationships for water-repellent and nearly wettable states of the soil.

Table 4
Soil water content, SWC ($m^3\ m^{-3}$), in the upper 5 cm of soil profile, water drop penetration time (WDPT), water repellency cessation time (WRCT), hydraulic conductivity (K(–2 cm)), sorptivity of both water (S_w(–2 cm)) and ethanol (S_e(–2 cm)), and repellency indices (RI, RI_c and RI_m), estimated at the experimental sites/subsites CI (Ciavolo, Italy), CSP17, CSP44 (Csólyospálos, Hungary), PW (Pwllpeiran, Wales, UK), SeN and SeS (Sekule, Slovakia) with N repetitions. SD: Standard deviation.

Site	Attribute	Minimum	Maximum	Arithmetic mean	SD	N
CI	SWC ($m^3\ m^{-3}$)	0.044	0.061	0.049	0.005	12
	WDPT (s)	1	100	14	28	13
	WRCT (s)	175	1248	558	350	9
	K(–2 cm) (m s^{-1})	9.85×10^{-7}	2.59×10^{-6}	1.74×10^{-6}	6.48×10^{-7}	9
	S_w(–2 cm) (m $s^{-1/2}$)	3.33×10^{-4}	5.89×10^{-4}	4.38×10^{-4}	8.96×10^{-5}	9
	S_e(–2 cm) (m $s^{-1/2}$)	4.16×10^{-4}	6.54×10^{-4}	5.14×10^{-4}	1.02×10^{-4}	4
	RI (–)	1.66	3.13	2.34	0.44	9
	RI_c (–)	1.38	3.83	2.36	0.59	36
	RI_m (–)	1.91	5.36	3.15	1.01	9
CSP17	SWC ($m^3\ m^{-3}$)	0.026	0.061	0.039	0.009	13
	WDPT (s)	1323	7680	3607	2041	13
	WRCT (s)	646	4114	2205	1258	9
	K(–2 cm) (m s^{-1})	3.3×10^{-7}	2.6×10^{-6}	1.2×10^{-6}	8.3×10^{-7}	9
	S_w(–2 cm) (m $s^{-1/2}$)	1.6×10^{-5}	1.5×10^{-4}	5.3×10^{-5}	4.3×10^{-5}	9
	S_e(–2 cm) (m $s^{-1/2}$)	2.1×10^{-3}	2.9×10^{-3}	2.4×10^{-3}	3.8×10^{-4}	9
	RI (–)	32.0	289.9	141.9	85.9	4
	RI_c (–)	n.d.	n.d.	n.d.	n.d.	–
	RI_m (–)	8.4	84.5	141.9	85.9	9
CSP44	SWC ($m^3\ m^{-3}$)	0.035	0.057	0.045	0.007	13
	WDPT (s)	422	13,630	2647	3672	13
	WRCT (s)	445	1913	1047	433	9
	K(–2 cm) (m s^{-1})	4.44×10^{-7}	2.94×10^{-6}	1.49×10^{-6}	8.45×10^{-7}	9
	S_w(–2 cm) (m $s^{-1/2}$)	1.40×10^{-5}	2.46×10^{-4}	7.59×10^{-5}	6.87×10^{-5}	9
	S_e(–2 cm) (m $s^{-1/2}$)	1.31×10^{-3}	2.90×10^{-3}	1.77×10^{-3}	7.65×10^{-4}	9
	RI (–)	14.09	246.15	78.78	67.96	4
	RI_c (–)	n.d.	n.d.	n.d.	n.d.	–
	RI_m (–)	5.97	14.4	10.11	3.38	9
PW	SWC ($m^3\ m^{-3}$)	0.39	0.55	0.48	0.05	10
	WDPT (s)	0	1	0.3	0.48	10
	WRCT (s)	0	1×10^{-9}	3×10^{-10}	4.83×10^{-10}	10
	K(–2 cm) (m s^{-1})	1.16×10^{-9}	8.13×10^{-8}	1.71×10^{-8}	2.39×10^{-8}	10
	S_w(–2 cm) (m $s^{-1/2}$)	3.40×10^{-5}	1.99×10^{-4}	1.10×10^{-4}	6.13×10^{-5}	10
	S_e(–2 cm) (m $s^{-1/2}$)	n.d.	n.d.	n.d.	n.d.	–
	RI (–)	n.d.	n.d.	n.d.	n.d.	–
	RI_c (–)	n.d.	n.d.	n.d.	n.d.	–
	RI_m (–)	0.001	0.001	0.001	0	10
SeN	SWC ($m^3\ m^{-3}$)	0.0010	0.0130	0.00450	0.428	8
	WDPT (s)	120	4500	1723	1610	12
	WRCT (s)	n.d.	n.d.	n.d.	n.d.	–
	K(–2 cm) (m s^{-1})	4.05×10^{-6}	9.42×10^{-5}	3.50×10^{-5}	3.70×10^{-5}	5
	S_w(–2 cm) (m $s^{-1/2}$)	1.14×10^{-3}	3.77×10^{-3}	2.39×10^{-3}	1.10×10^{-3}	5
	S_e(–2 cm) (m $s^{-1/2}$)	4.27×10^{-4}	2.23×10^{-3}	1.14×10^{-3}	6.77×10^{-4}	5
	RI (–)	0.993	17.2	5.427	4.021	25
	RI_c (–)	n.d.	n.d.	n.d.	n.d.	–
	RI_m (–)	n.d.	n.d.	n.d.	n.d.	–
SeS	SWC ($m^3\ m^{-3}$)	0.0023	0.0234	0.01016	0.756	10
	WDPT (s)	1	6883	664	1728	16
	WRCT (s)	n.d.	n.d.	n.d.	n.d.	–
	K(–2 cm) (m s^{-1})	1.25×10^{-6}	8.13×10^{-5}	1.80×10^{-5}	2.10×10^{-5}	14
	S_w(–2 cm) (m $s^{-1/2}$)	3.60×10^{-5}	1.28×10^{-3}	3.42×10^{-4}	3.42×10^{-4}	16
	S_e(–2 cm) (m $s^{-1/2}$)	9.97×10^{-4}	5.66×10^{-3}	2.85×10^{-3}	1.82×10^{-3}	11
	RI (–)	1.52	306.7	57.73	77.300	176
	RI_c (–)	n.d.	n.d.	n.d.	n.d.	–
	RI_m (–)	n.d.	n.d.	n.d.	n.d.	–

where C_2 is the coefficient of the quadratic term of the parabola when the cumulative infiltration data are fitted as a function of the square roort of time and A is a dimensionless coefficient that's value is relating the van Genuchten retention parameters for a given soil to suction at the infiltration surface and the infiltrometer disk radius.. Eq. (2) was used to estimate the soil hydraulic conductivity K(–2 cm) in this study. The values of A were obtained from the Minidisk Infiltrometer User's Manual (Decagon Devices, 2012).

In the standard method of estimating the repellency index, RI (–), S_e and S_w were measured in pairwise arrangements and the standard repellency index RI was calculated as follows (Hallett et al., 2001):$RI = 1.95\ S_e\ /\ S_w$(3)

In the second method of estimating the repellency index, the combination of all the ethanol (S_e (m $s^{-1/2}$)) and water sorptivities (S_w (m $s^{-1/2}$)) was used to calculate a combined repellency index, RI_c (–), i.e., m × n values of RI (–) were calculated from m values of S_w (m $s^{-1/2}$) and n values of S_e (m $s^{-1/2}$) (Pekárová et al., 2015).

In the third method of estimating the repellency index, the water sorptivity for water-repellent state of soil, S_{wh} (m $s^{-1/2}$), and the water sorptivity for nearly wettable state of soil, S_{ww} (m $s^{-1/2}$), were calculated, respectively, from the shallower and steeper parts of hockey-stick-like relationship (Fig. 3). This relationship was used to calculate the modified repellency index RI_m (–) (Alagna et al., 2017; Sepehrnia et al., 2016).

The persistence of SWR was assessed by both water drop penetration time (WDPT (s)) and water repellency cessation time (WRCT (s))

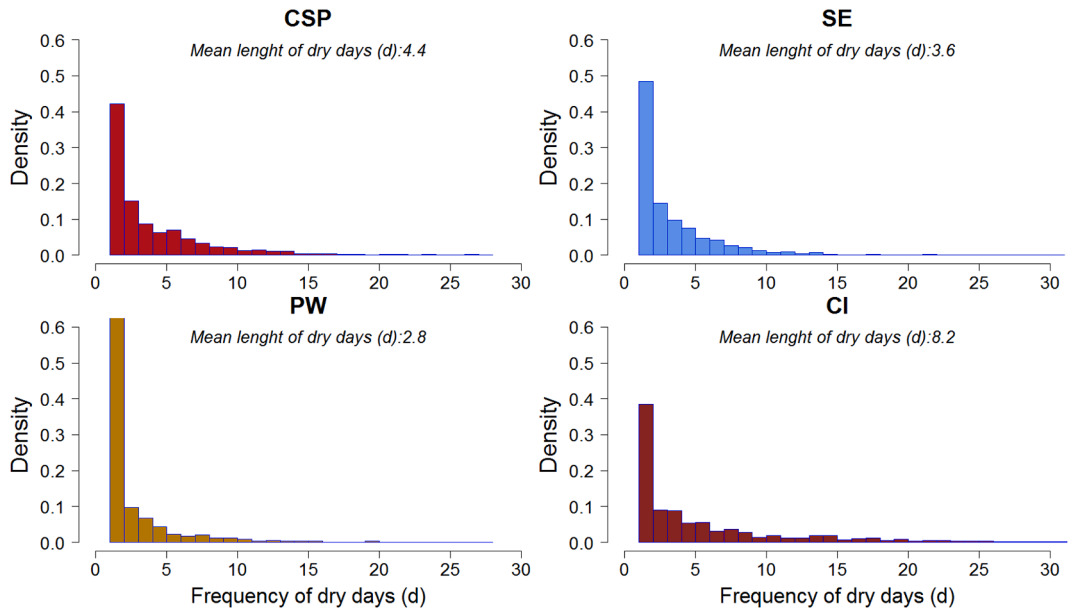

Fig. 4. Frequency of dry day lengths at CSP (Csólyospálos, HU), SE (Sekule, SK), PW (Pwllpeiran, UK) and CI (Ciavolo, IT) sites between 1st of April and 31st of October.

(Lichner et al., 2013). The WDPT test involves placing a 50 ± 5 μL water drop from a standard medicine dropper or pipette on the soil surface and recording the time of its complete penetration (Doerr, 1998). A standard droplet release height of approximately 10 mm above the soil surface was used to minimize the cratering effect on the soil surface. As the preliminary actual SWC of the PW site was high, we carried out a laboratory WDPT measurement on dry samples in five repetitions to prove the persistence of water repellency. A classification for the repellency indices (*RI* and RI_c) based on the widely applied classification for WDPT (Dekker et al., 2009) was proposed by Iovino et al. (2018). WRCT was estimated from the intersection of two straight lines, representing the two stages of infiltration (Fig. 3) (Lichner et al., 2013).

2.3. Statistical analyses

Daily, monthly and yearly aggregated precipitation, minimum, maximum temperature database were analysed between 1980 and 2017 to estimate climate indexes such as rainfall seasonality, aridity index and to determine the multi-year average annual temperature, summer temperature, annual precipitation and summer precipitation values which are reported in Table 1. For determining the aridity categories of the sites, the De Martonne-Gottmann index (b) was calculated at each site (De Martonne, 1942) using the following categories: $5 \leq b \leq 14$: arid, $15 \leq b \leq 19$: semi-arid, $20 \leq b \leq 29$: sub-humid and $30 \leq b \leq 59$: humid. To describe the seasonality of the precipitation, the rainfall seasonality index (SI_P) were calculated, where $-0.13 \leq SI_P \leq 0.13$ category describes uniform distribution, more negative values show wetter winters than summers, while more positive values mean wetter summers (Walsh and Lawler, 1981). To complete the study with further meteorological analyses, the length of dry spells (number of consecutive dry days) were summarized and ordered. Rainy days got zero values and were excluded from the dry spell length calculations, and the number of the dry days were added until the next precipitation event. This approach helped to demonstrate the severity of water deficit periods. These indexes and calculations were used to described and distinguish the sites' climatic circumstances and differences.

Measured WDPT and WRCT values of the measuring quadrat were analysed by using percent exceedance probability distributions, approximated as $[m/(n + 1)] \times 100$, where m is a rank order of each estimate, with $m = 1$ as the largest and $m = n$ for the lowest, with n being the number of available data (number of available data is shown in Table 4). These analyses provide the opportunity to establish the severity of SWR at each site.

For establishing further relationships between the measured soil chemical ($CaCO_3$, organic carbon contents and pH) and hydrological properties (such as soil water content, WDPT, hydraulic conductivity, sorptivity and repellency index) at the sites we applied Pearson's correlation and scatterplot correlation matrix for characterizing the differences and similarities. Different combinations of variables for different locations were selected, because not all sites had the same number of measured hydrological properties (see in Table 4, last column), because, for instance, if a site was not water repellent there was no available *RI* or S_e data. PW site provided soil texture measurements from each soil hydrology measuring cell, but these measurements were not available for every point of the quadrat of other sites.

R Studio (R Studio Team, 2016) was used for statistical computing and graphical visualization.

3. Results and discussion

The SWC ($m^3\ m^{-3}$), of the upper 5 cm of soil profile had the highest values at the PW site, while other sites' water contents were below 5% (Table 4). At the PW site WDPT measurements were carried out on dried samples resulting in $WDPT_P = 0.7 \pm 0.2$ s, which confirmed the PW site to be non-repellent. There was high variability between and within sites and land covers in WDPT, field hydraulic conductivity(K)(–2 cm), both water, S_w(–2 cm) and ethanol sorptivity, S_e(–2 cm), and repellency index prior to the infiltration experiment. For instance, the highest variability of WDPT was recorded at the CSP site, with the greatest average values at the CSP17 site. However, the maximum WDPT value was observed for the CSP44 site. The cumulative infiltration of water showed a hockey-stick-like relationship over time (Fig. 3) at the CSP and CI sites, where the water repellent (S_{wh}) and wettable (S_{ww}) state of soil were demonstrated by different infiltration rates. This relationship was not observed at the SE and PW sites, although the soil physical properties were similar: SE *vs* CSP and PW *vs* CI (Table 2), but there are some differences in their pH values, soil organic matter, bulk density and $CaCO_3$ contents and vegetation abundance. Therefore, the differences were more likely caused by the interactions between climate, soil chemical properties and vegetation cover.

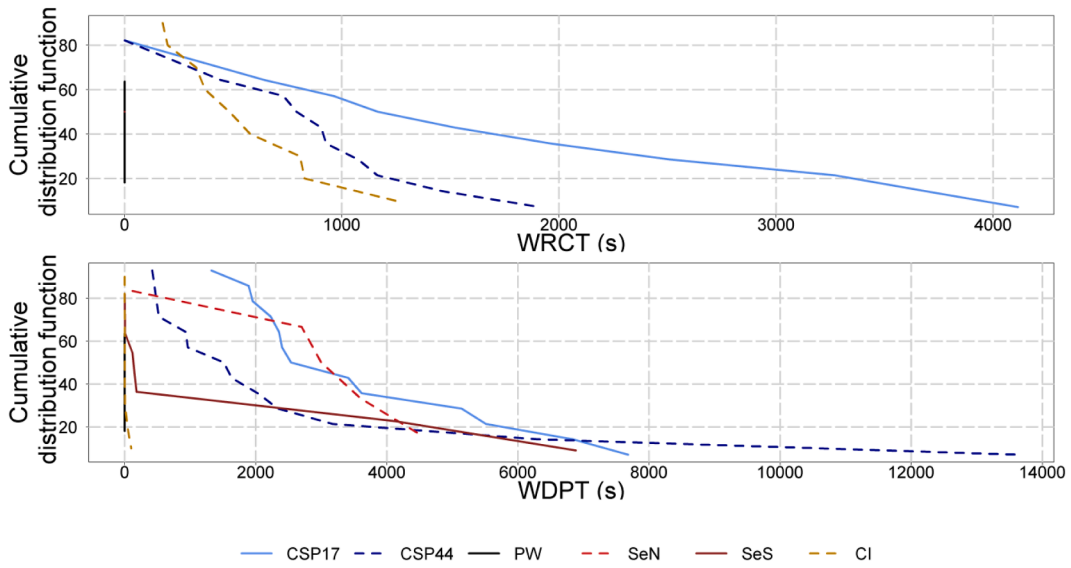

Fig. 5. Exceedance probability distribution functions (%) of WRCT and WDPT values at experimental sites/sub-sites CI (Ciavolo, Italy), CSP17, CSP44 (Csólyospálos, 17 and 44 years abandoned fields in Hungary, respectively), PW (Pwllpeiran, Wales, UK), SeN and SeS (Sekule, under natural and synanthropized vegetation in Slovakia, respectively).

3.1. Effect of climate and seasonal field conditions on SWR

Analyses of the frequency of dry days (Fig. 4) during the summer half year (between 1st of April and 31st of October) showed that the PW site had the shortest dry spell length, 2.9 d across years, with the longest drought period 31 d during the period 1980 to 2017. The SE site's average dry spell length was 3.6 d, and the longest dry spell was 37 d. The CSP site experienced more arid conditions, with a 4.7 d average length of day period across investigated years. The longest dry period here lengthened to 50 d, whilst it was 99 d at CI. The Mediterranean site's average annual dry day length was 4.9 d, while it was 8.2 during the summer term. According to these analyses, the chance of precipitation is 2.5 times greater at PW than at other sites, which means around 62% of the year is rainy, compared to 32–36% at other sites. This estimate corresponds to the annual climatic conditions (see in Table 1, and Fig. 2). The CSP and CI sites showed the highest chance of dry periods; their De Martonne-Gottman aridity (*b*, De Martonne, 1942) categories are semi-arid and arid ($b = 14.4 \pm 6.5$ and 10.6 ± 2.9) and also the precipitation is relatively low ($\sim 310 \pm 134$ and $\sim 160 \pm 64$ mm, respectively) during the growing season, which is associated with high average maximal summer temperatures ($\sim 36 \pm 2$ and $\sim 37 \pm 3$ °C, respectively). Owing to the high temperature and rainless periods at the CSP, SE and CI sites, the soil moisture content was low, below 0.05 m^3 m^{-3} on average (see SWC in Table 4). This low, near zero, SWC value could considerably decrease and in some cases halt the rate of evaporation, as a dry surface layer functions as an impeding layer. Thus, the dry surface layer is able to significantly diminish the net evaporative moisture loss; according to Rye and Smettem (2017) the near surface layer's evaporative losses decreased by 70–80 % compare to a wettable control soil. Lichner et al. (2020) found that a 2 cm thick layer of duff or water repellent sand saved up to 58–59% of water from evaporation in a clay loam soil and sand soil, respectively. The length of the rainless period has been reported as being positively correlated with the severity of SWR (de Jonge et al., 1999; Doerr et al., 2000), which corresponds to our findings; the maximum length of the dry period was highest at the CSP and CI sites. Considering the wetting–drying history three months before the measurements, CI site had the lowest amount of precipitation (~17 mm), after SE and CSP sites (~161 and ~162 mm, respectively) and PW (~387 mm). To explore the chances of finding strong or extreme water repellent points at the sites in more detail, cumulative distribution functions (Fig. 5) were calculated, which demonstrate the exceedance probability of WRCT and WDPT values. In addition, the importance of vegetation cover was investigated for the CSP and SE sites.

3.2. Effect of vegetation on SWR

In terms of WRCT, which is estimated from the intersection of the linearized hydrophobic and hydrophilic sections of the water infiltration curve, the CSP44 site showed the greatest WRCT (Table 4, Fig. 5), followed by CSP17 site. This suggests that strongly synanthropized vegetation or poor grassland dominated by perennial weedy grass and annual grasses has enhanced the SWR at the CSP site. The SE and PW sites did not exhibit hydrophobic stage of the infiltration, therefore no S_{wh} values were estimated. Thus, the chance of finding an extremely strong water repellent measuring point (WDPT > 3600 s), was ~20% at the CSP44 site, ~26% at SeS, and above 40% at the CSP17 and SeN sites, whereas it was ~0% at PW and CI. The natural vegetation at the SE site showed much higher SWR values than under synanthropized vegetation, which contradicts what was found at the CSP site. This paradox can be resolved by attributing more influence to climate, and the length of dry spells in particular, in developing SWR. However, the greatest WDPT values were measured at CSP44 (13630 s, Table 4), which has more natural grassland species similar to SeN. This also suggests that the effect of the climate factor on SWR could be even greater than the effect of the vegetation cover, which corresponds to the fact that the water repellency is not a static soil property and has a strong seasonal variance (Dekker et al., 2009). For instance, the entire topsoil can dry out and become water repellent during prolonged hot and dry periods, which induces incomplete wetting during subsequent rainfall events. According to Täumer et al. (2005) the total effective cross section area is being reduced to 20% to 40% therefore the potential rate of infiltration is much smaller than would result from the soil texture. A previous study (Sándor et al., 2015) at CSP17 site, when the site was 12 years abandoned, showed that SWR was not a function of the organic matter type, but rather caused by the large quantity of non-degraded organic compounds of the local vegetation. In this case, the SWR could be attributed to the drought related withering and degradation of vegetation, rather than the actual constituents of "fresh" vegetation.

3.3. Correlations between soil hydrological properties

The correlation scatterplot analyses highlight the connections

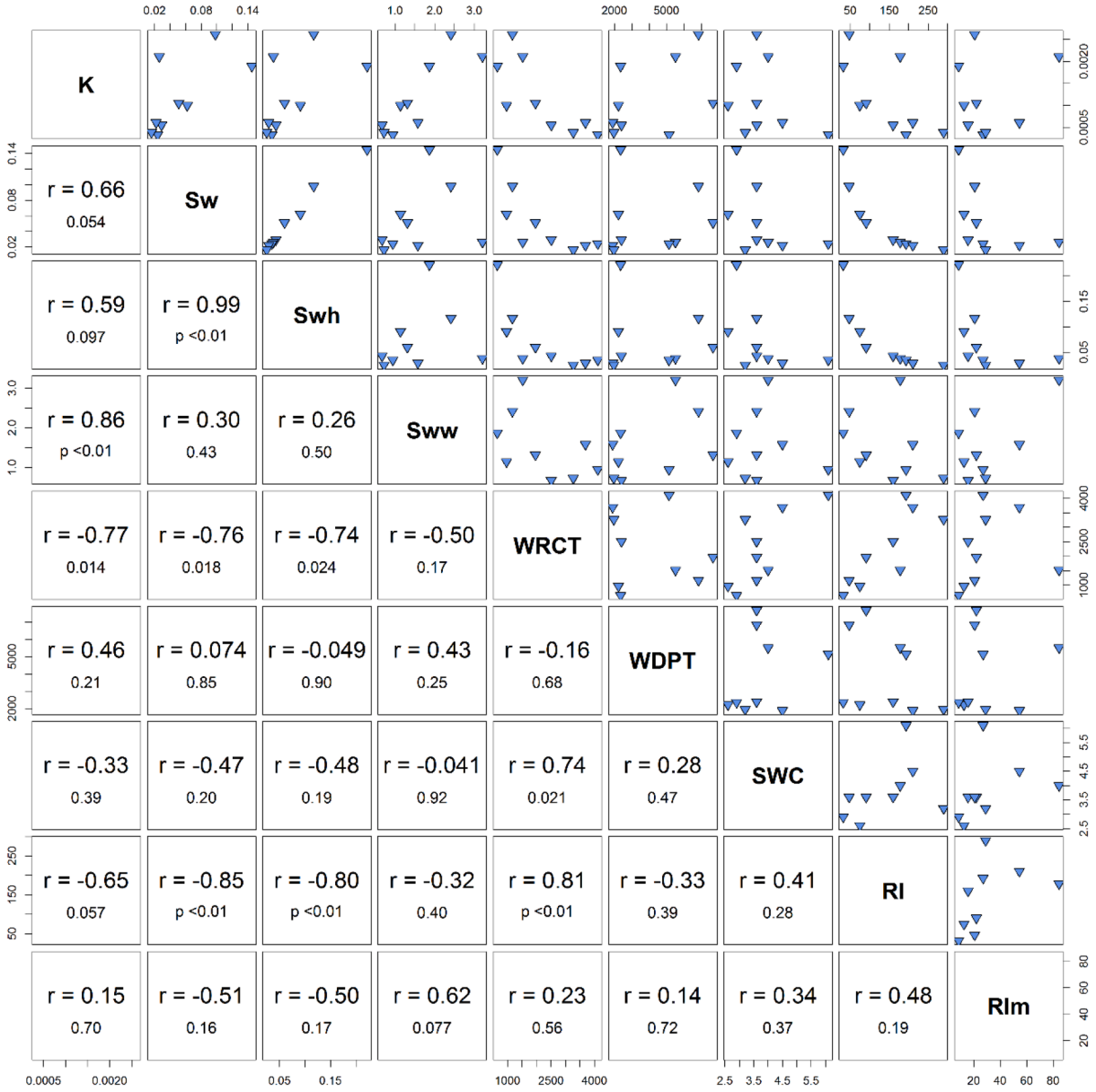

Fig. 6. Scatterplot Pearson-correlation matrix of hydrophysical properties at the CSP17 (Csólyospálos, Hungary) site, where K: field unsaturated hydraulic conductivity; S_w: field water sorptivity; S_{wh}: water sorptivity of hydrophobic soil state; S_{ww}: water sorptivity of nearly wettable soil state; WRCT: water repellency cessation time; WDPT: water drop penetration time, SWC: soil water content, RI and RI_m: repellency indices.

2

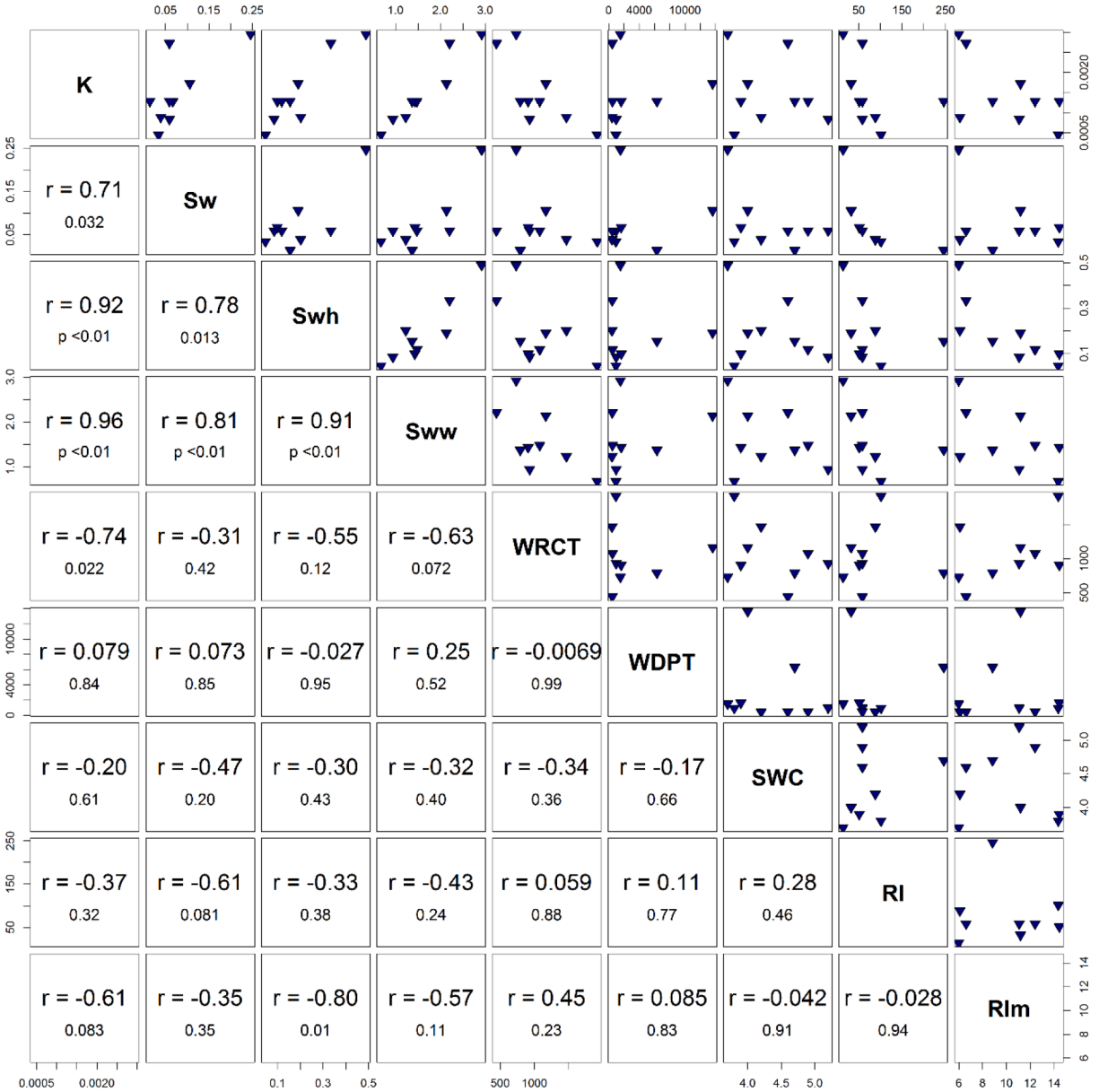

Fig. 7. Scatterplot Pearson-correlation matrix of hydrophysical properties at CSP44 (Csólyospálos, Hungary) site, where *K*: field unsaturated hydraulic conductivity; S_w: field water sorptivity; S_{wh}: water sorptivity of hydrophobic soil state; S_{ww}: water sorptivity of nearly wettable soil state; WRCT: water repellency cessation time; WDPT: water drop penetration time, SWC: soil water content, *RI* and RI_m: repellency indices.

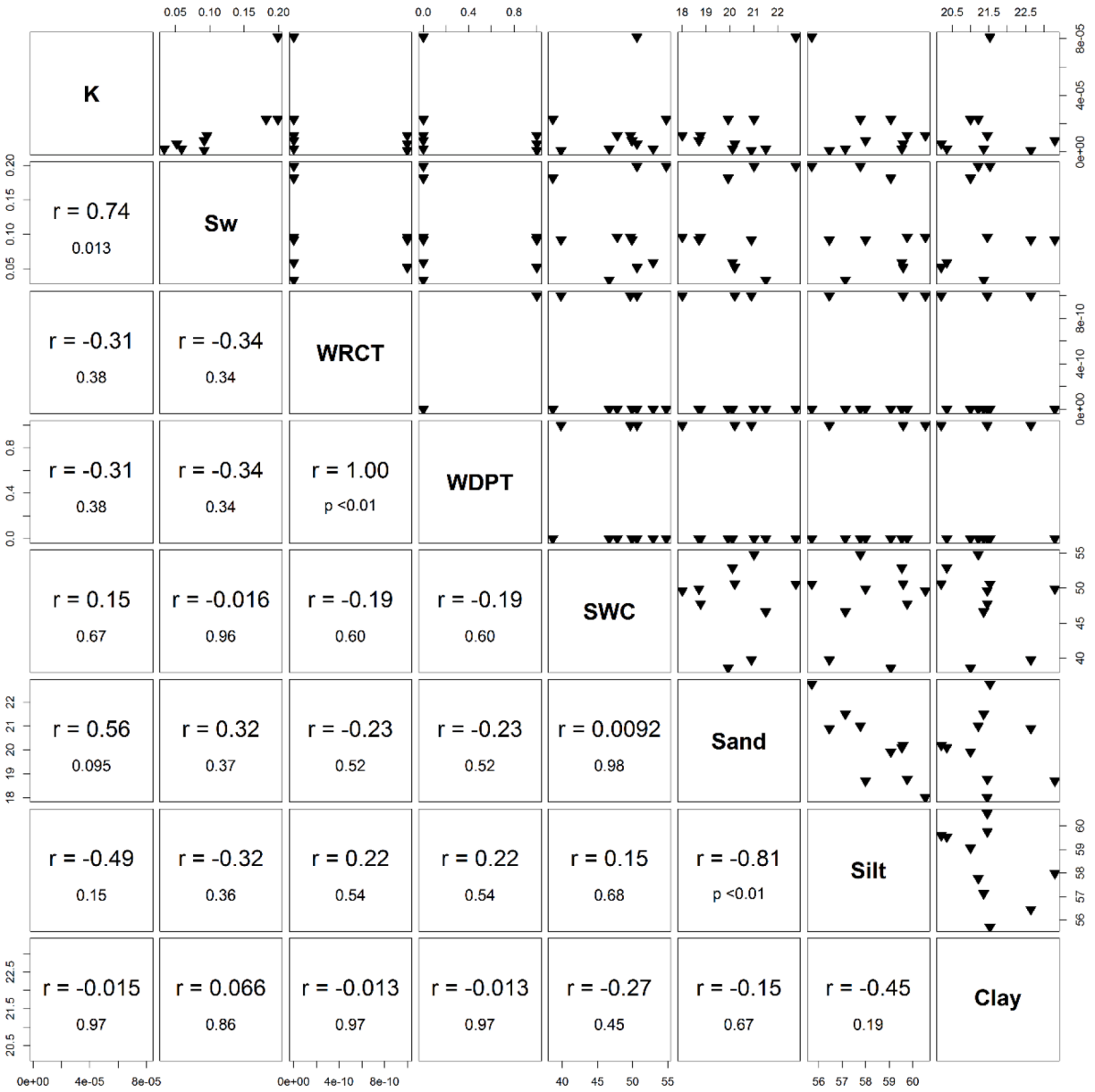

Fig. 8. Scatterplot Pearson-correlation matrix of hydrophysical properties at PW (Pwllpeiran, Wales, UK) site, where *K*: field unsaturated hydraulic conductivity; S_w: field water sorptivity; WRCT: water repellency cessation time; WDPT: water drop penetration time, SWC: soil water content, and Sand, Silt and Clay contents.

between the different measured values and variables (Figs. 6–11), where soil hydraulic conductivity, *K*, is positively correlated with all the sorptivity values (S_w, S_{wh}, S_{ww}) for all the sites. Values for *K* have a negative correlation with WRCT at all sites, and with *RI* and WDPT at most of the sites. Also, a slight negative correlation was found between *K* and moisture content. Although *K* was relatively more variable at SE and PW sites with coefficients of variation (CV) in the range 1.05 to 1.39, the spatial heterogeneity of *K* was within the values reported in literature, where, for example, *K* reached three orders of magnitude difference within the pedon scale at CSP site (Sándor et al., 2015). The repellency index mostly demonstrates a negative correlation with sorptivity (S_w, S_{wh} and S_{ww}) values. In general, WRCT and WDPT positively and significantly correlates with S_w and S_{wh} (*r* is between 0.28 and 0.81), but a negative correlation was found with the water sorptivity of nearly wettable soil state, S_{ww}, at the CI site ($r = -0.50$ and -0.37, respectively) (Fig. 11). At the PW site, the soil texture was also compared with the infiltration values (Fig. 8), where only the sand content showed a high positive correlation ($r = 0.56$) with hydraulic conductivity, whilst the silt and clay content negatively correlated ($r = -0.49$ and $r = -0.002$, respectively) with it. Clay content was negatively correlated with SWC values (Fig. 8). Regardless, our moisture content measurements reveal generally negative correlations with SWR related values (e.g. Fig. 9), although SWC alone is not a reliable predictor for the appearance and disappearance of SWR (e.g. Müller et al., 2014) owing to its limitation and high seasonal variability and spatial heterogeneity.

Overall, there is a general existence of a correlation between hydrophysical properties (*K* and sorptivity in the early stage of infiltration, S_w and S_{wh}) and repellency indices (*RI*, RI_c and RI_m). However correlations are not always significant, but the sign is in most cases negative (always for *S*). This is meaningful as one should expect that infiltration is prevented in SWR soils. As our regional scale investigations demonstrate, to establish the SWR risk of an area, meteorological factors, soil properties and land cover type also play key roles alongside the SWC.

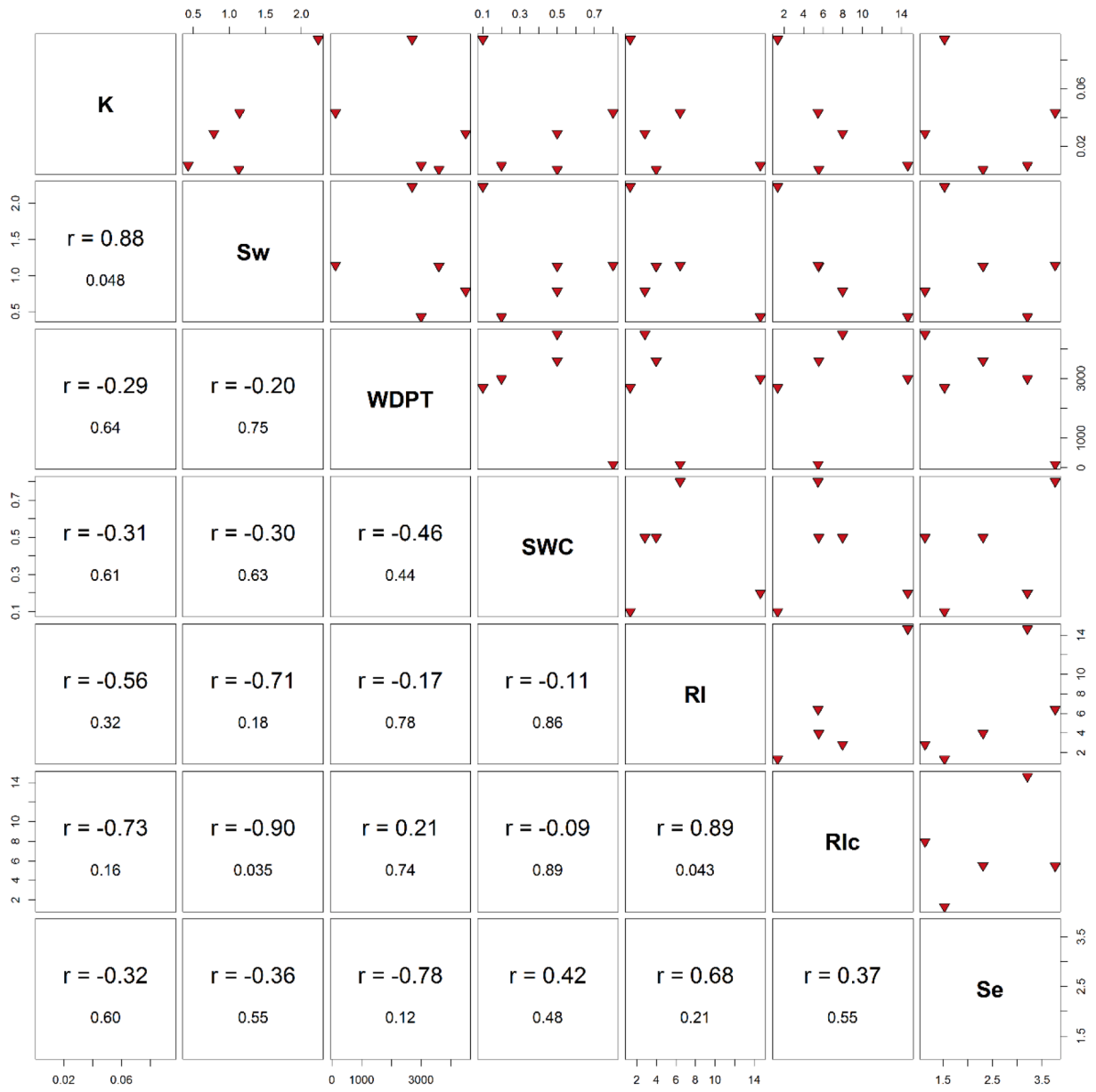

Fig. 9. Scatterplot Pearson-correlation matrix of hydrophysical properties at SeN (Sekule, Slovakia) site, where K: field unsaturated hydraulic conductivity; S_w: field water sorptivity; WDPT: water drop penetration time, SWC: soil water content, RI and RI_c: repellency indices; S_e: field ethanol sorptivity.

4. Conclusions

Separate and combined effects of two main factors (climate and soil texture) on SWR were investigated at four sites from different climatic and soil regions across Europe. Based on our results, sites with finer texture soil under humid climate are unlikely to be water repellent. The PW site shows no signs of SWR thus no factor known to cause repellency is present or strong enough to induce repellency. Regions with coarser texture soils (CSP and SE sites) with high or, conversely, low organic matter content and regions with drier climatic zones (CI site) characterized by longer dry periods have a greater likelihood of containing water repellent soils. Hydraulic conductivity showed a positive correlation with all the sorptivities (S_w, S_{wh}, S_{ww}), but was generally negatively correlated with the repellency index, WDPT and WRCT. The fact that climatic or soil textural differences could indicate differences in SWR despite the variations in either the pH or the soil organic matter content demonstrates that climate and soil texture are two of the main factors influencing SWR. This conclusion was supported by the finding that climatic factors can override or supress the impact of vegetation on SWR as it was observed at PW site where SWR was not induced under grass cover even during or after long dry spells.

Our findings support identifying localized non-repellent areas (such as PW) and distinguishing them from potentially water repellent places, providing opportunities to develop site-specific solutions. If a soil has coarse texture (SE site) or a high frequency of water stress periods during the vegetation period (CI site) it could induce slight SWR, whilst the combination of these factors could cause strong and some places extreme water repellent circumstances (CSP site). Within the current study the SWR characteristics of the natural, perennial grass dominated surface cover provided more favourable conditions under strong and extreme water repellent conditions at CSP. Therefore, there is an increasing need to take SWR into account to a greater extent in grassland ecosystems. There are recent initiatives to simulate the soil–water dynamics of water repellent soils (e.g. Brown et. al., 2018), where the phenomena of preferential flow is also included. However, the SWR is more complex, as it has effect on surface runoff, nutrient loss, soil

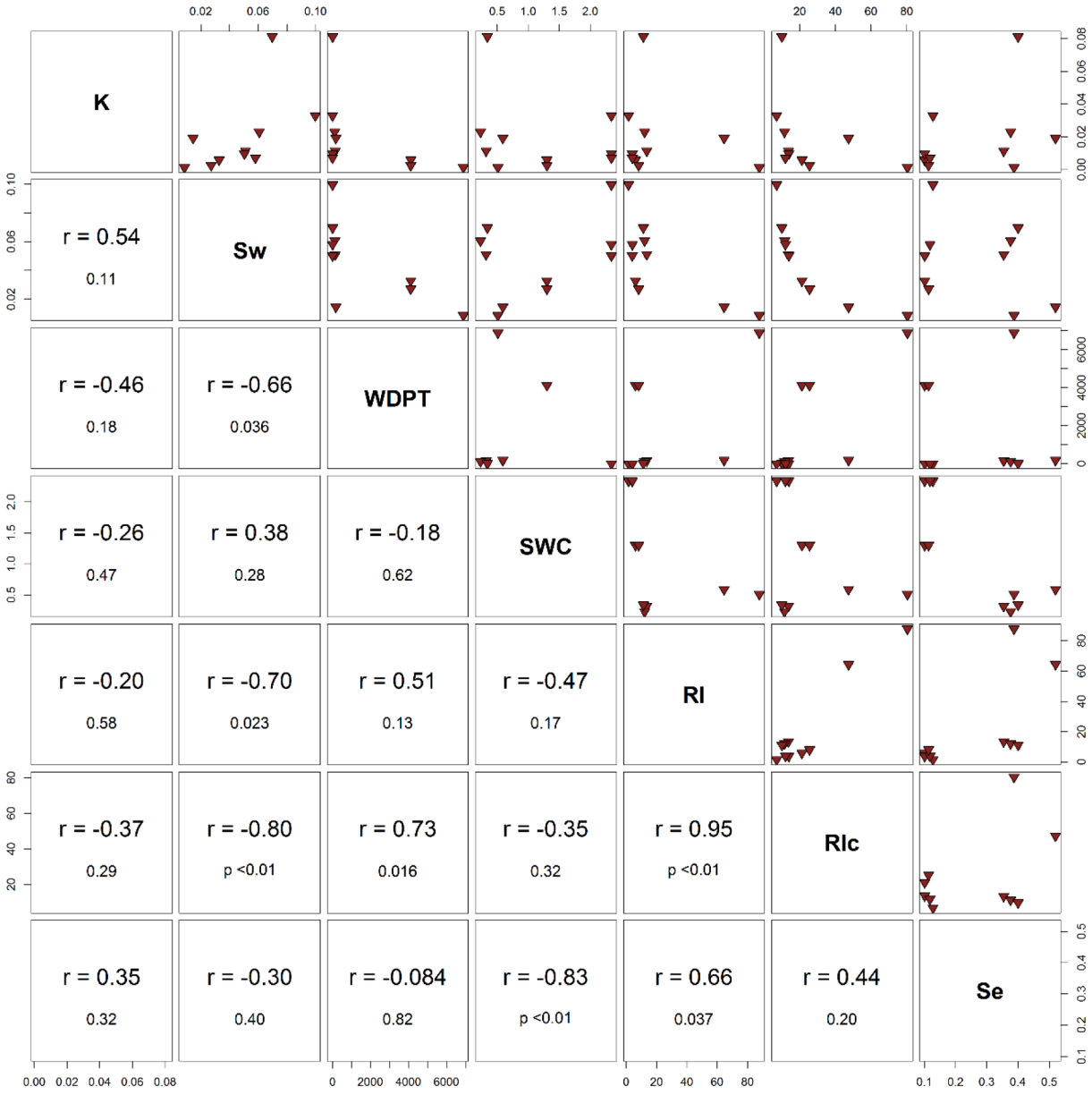

Fig. 10. Scatterplot Pearson-correlation matrix of hydrophysical properties at SeS (Sekule, Slovakia) site, where K: field unsaturated hydraulic conductivity; S_w: field water sorptivity; WDPT: water drop penetration time, SWC: soil water content, RI and RI_c: repellency indices; S_e: field ethanol sorptivity.

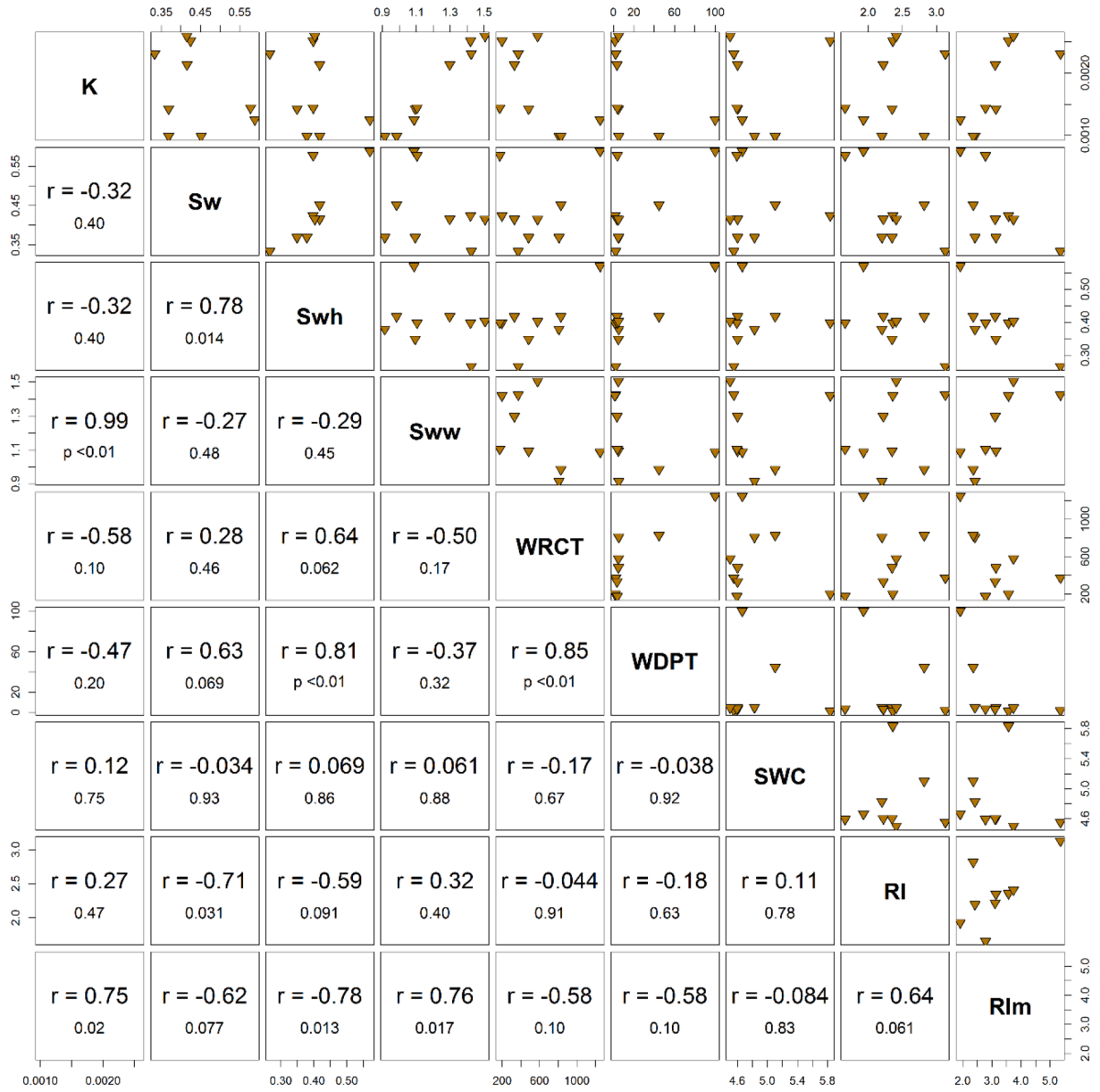

Fig. 11. Scatterplot Pearson-correlation matrix of hydrophysical properties at CI (Ciavolo, Italy) site, where *K*: field unsaturated hydraulic conductivity; S_w: field water sorptivity; S_{wh}: water sorptivity of hydrophobic soil state; S_{ww}: water sorptivity of nearly wettable soil state; WRCT: water repellency cessation time; WDPT: water drop penetration time, SWC: soil water content, RI and RI_m: repellency indices.

nitrogen and carbon pools, and productivity, as well as biodiversity. Future study will focus on modelling SWR phenomenon what could help us to determine potentially water repellent areas and define the most sustainable grassland community of each risk zone in order to optimize their water management and increase their productivity and carbon sink potential.

Declaration of Competing Interest

The authors declare that they have no known competing financial interests or personal relationships that could have appeared to influence the work reported in this paper.

Acknowledgements

This work was supported by the Slovak Scientific Grant Agency VEGA Project 2/0020/20, the Slovak Research and Development Agency Project APVV-15-0160, the János Bolyai Research Scholarship of the Hungarian Academy of Sciences, the Széchenyi 2020 programme, and the European Regional Development Fund, and the Hungarian Government (GINOP-2.3.2-15-2016-00028). This publication is a result of the project implementation ITMS 26220120062 Centre of excellence for the Integrated River Basin Management in the Changing Environmental Conditions, supported by the Research & Development Operational Programme funded by the ERDF and the EIG JC2019-074 Soil Eco-Technology to Recover Water Storage in disturbed Forests. The extension of the study to the United Kingdom was funded by The Stapledon Memorial Trust and the UK Biotechnology and Biological Sciences Research Council (grant no. BBS/E/W/0012843C).

References

Alagna, V., Iovino, M., Bagarello, V., Mataix-Solera, J., Lichner, L., 2017. Application of minidisk infiltrometer to estimate water repellency in Mediterranean pine forest soils. J. Hydrol. Hydromech. 65, 254–263.

Alagna, V., Iovino, M., Bagarello, V., Mataix-Solera, J., Lichner, L., 2018. Alternative analysis of transient infiltration experiment to estimate soil water repellency. Hydrol. Process. 33, 661–674.

Alaoui, A., Caduff, U., Gerke, H.H., Weingartner, R., 2011. Preferential flow effects on infiltration and runoff in grassland and forest soils. Vadose Zone J. 10, 367–377.

Bachmann, J., Horton, R., van der Ploeg, R.R., 2001. Isothermal and nonisothermal evaporation from four sandy soils of different water repellency. Soil Sci. Soc. Am. J. 65, 1599–1607.

Beven, K., Germann, P., 2013. Macropores and water flow in soils revisited. Water Resour. Res. 49, 3071–3092.

Bisdom, E.B.A., Dekker, L.W., Schoute, J.F.T., 1993. Water repellency of sieve fractions from sandy soils and relationships with organic material and soil structure. Geoderma 56, 105–118.

Brown, H., Carrick, S., Müller, K., Thomas, S., Sharp, J., Cichota, R., Holzworth, D., Clothier, B., 2018. Modelling soil-water dynamics in the rootzone of structured and water-repellent soils. Comput. Geosci. 113, 33–42. https://doi.org/10.1016/j.cageo.2018.01.014.

Clark, E.V., Zipper, C.E., 2016. Vegetation influences near-surface hydrological characteristics on a surface coal mine in eastern USA. Catena 139, 241–249.

Clothier, B.E., Vogeler, I., Magesan, G.N., 2000. The breakdown of water repellency and solute transport through a hydrophobic soil. J. Hydrol. 231–232, 255–264.

Decagon Devices, 2012. Mini Disk Infiltrometer – User's Manual. Version 10. Decagon Devices, Inc., Pullman.

de Jonge, L.W., Jacobsen, O.H., Moldrup, P., 1999. Soil water repellency: effects of water content, temperature, and particle size. Soil Sci. Soc. Am. J. 63, 437–442.

Dekker, L.W., Ritsema, C.J., 1994. How water moves in a water repellent sandy soil: 1. Potential and actual water repellency. Water Resour. Res. 30, 2507–2517.

Dekker, L.W., Ritsema, C.J., 1996. Preferential flow paths in a water repellent clay soil with grass cover. Water Resour. Res. 32, 1239–1249.

Dekker, L.W., Ritsema, C.J., Oostindie, K., Moore, D., Wesseling, J.A., 2009. Methods for determining soil water repellency on field-moist samples. Water Resour. Res. 45, W00D33.

De Martonne, E., 1942. Nouvelle carte mondiale de l'indice d'aridité. Annales de Géographie 51, 242–250.

Diehl, D., Bayer, J.V., Woche, S.K., Bryant, R., Doerr, S.H., Schaumann, G.E., 2010. Reaction of soil water repellency to artificially induced changes in soil pH. Geoderma 158, 375–384.

Diehl, D., 2013. Soil water repellency: Dynamics of heterogeneous surfaces. Colloids and Surfaces A: Physicochem. Eng. Aspects 432, 8–18.

Doerr, S.H., 1998. On standardizing the "Water Drop Penetration Time" and the "Molarity of an Ethanol Droplet" techniques to classify soil hydrophobicity: a case study using medium textured soils. Earth Surf. Proc. Land. 23, 663–668.

Doerr, S.H., Shakesby, R.A., Walsh, R.P.D., 2000. Soil water repellency: its causes, characteristics and hydrogeomorphological significance. Earth Sci. Rev. 51, 33–65.

Doerr, S.H., Moody, J.A., 2004. Hydrological effects of soil water repellency: on spatial and temporal uncertainties. Hydrol. Process. 18, 829–832.

EUROSTAT, Statistical Service of the European Union https://ec.europa.eu/eurostat/statistics-explained/index.php/Land_cover_statistics#Land_cover_in_the_EU.

Fér, M., Leue, M., Kodešová, R., Gerke, H.H., Ellerbrock, R.H., 2016. Droplet infiltration dynamics and soil wettability related to soil organic matter of soil aggregate coatings. J. Hydrol. Hydromech. 64, 111–120.

Fischer, C., Tischer, J., Roscher, C., Eisenhauer, N., Ravenek, J., Gleixner, G., Attinger, S., Jensen, B., de Kroon, H., Mommer, L., Scheu, S., Hildebrandt, A., 2015. Plant species diversity affects infiltration capacity in an experimental grassland through changes in soil properties. Plant Soil 397, 1–16.

Fischer, E.M., Schär, C., 2010. Consistent geographical patterns of changes in high-impact European heatwaves. Nat. Geosci. 3, 398–403.

Goebel, M.-O., Bachmann, J., Woche, S.K., Fischer, W.R., 2005. Soil wettability, aggregate stability, and the decomposition of soil organic matter. Geoderma 128, 80–93.

Goebel, M.-O., Bachmann, J., Reichstein, M., Janssens, I.A., Guggenberger, G., 2011. Soil water repellency and its implications for organic matter decomposition – is there a link to exteme climatic events? Glob. Change Biol. 17, 2640–2656.

Hallett, P.D., Young, I.M., 1999. Changes to water repellence of soil aggregates caused by substrate-induced microbial activity. Eur. J. Soil Sci. 50, 35–40.

Hallett, P.D., Baumgartl, T., Young, I.M., 2001. Subcritical water repellency of aggregates from a range of soil management practices. Soil Sci. Soc. Am. J. 65, 184–190.

Imeson, A.C., Verstraten, J.M., van Mulligen, E.J., Sevink, J., 1992. The effects of fire and water repellency on infiltration and runoff under Mediterranean type forest. Catena 19, 345–361.

Iovino, M., Pekárová, P., Hallett, P.D., Pekár, J., Lichner, L., Mataix-Solera, J., Alagna, V., Walsh, R., Raffan, A., Karsten, S., K., Rodný, M.,, 2018. Extent and persistence of soil water repellency induced by pines in different geographic regions. J. Hydrol. Hydromech. 66, 360–368. https://doi.org/10.2478/johh-2018-0024.

IPCC, 2019. Climate Change and Land: an IPCC special report on climate change, desertification, land degradation, sustainable land management, food security, and greenhouse gas fluxes in terrestrial ecosystems [P.R. Shukla, J. Skea, E. Calvo Buendia, V. Masson-Delmotte, H.-O. Pörtner, D. C. Roberts, P. Zhai, R. Slade, S. Connors, R. van Diemen, M. Ferrat, E. Haughey, S. Luz, S. Neogi, M. Pathak, J. Petzold, J. Portugal Pereira, P. Vyas, E. Huntley, K. Kissick, M. Belkacemi, J. Malley, (eds.)]. In press.Kneitel, J., 2010. Successional Changes in Communities. Nature Education Knowledge 3, 10– 41.

Kottek, M., Grieser, J., Beck, C., Rudolf, B., Rubel, F., 2006. World Map of the Köppen-Geiger climate classification updated. Meteorologishe Zeitschrift 15, 259–263.

Lichner, L., Babejová, N., Dekker, L.W., 2002. Effects of kaolinite and drying temperature on the persistence of soil water repellency induced by humic acids. Rostlinná Výroba 48, 203–207.

Lichner, L., Holko, L., Zhukova, N., Schacht, K., Rajkai, K., Fodor, N., Sándor, R., 2012. Plants and biological soil crust influence the hydrophysical parameters and water flow in an aeolian sandy soil. J. Hydrol. Hydromech. 60, 309–318.

Lichner, L., Hallett, P.D., Drongová, Z., Czachor, H., Kovacik, L., Mataix-Solera, J., Homolák, M., 2013. Algae influence hydrophysical parameters of a sandy soil. Catena 108, 58–68.

Lichner, L., Alagna, V., Iovino, V., Laudicina, V.A., Novák, V., 2020. Evaporation from soils of different texture covered by layers of water repellent and wettable soils. Biologia 75, 865–872.

Lozano-Baez, S.E., Cooper, M., de Barros Ferraz, S.F., Ribeiro Rodrigues, R., Lassabatere, L., Castellini, M., Di Prima, S., 2020. Assessing water infiltration and soil water repellency in Brazilian Atlantic forest soils. Applied Sciences 10, 1950. https://doi.org/10.3390/app10061950.

Mao, J.F., Nierop, K.G.J., Rietkerk, M., Damsté, J.S.S., Dekker, S.C., 2016. The influence of vegetation on soil water repellency-markers and soil hydrophobicity. Sci. Total Environ. 566–567, 608–620.

McKissock, I., Walker, E.L., Gilkes, R.J., Carter, D.J., 2000. The influence of clay type on reduction of water repellency by applied clays: a review of some West Australian work. J. Hydrol. 231–232, 323–332.

Meehl, G.A., Stocker, T.F., Collins, W.D., 2007. Global climate projections. In: Solomon, S., Qin, D., Manning, M. (Eds.), Climate change: The Physical Science Basis. Contribution of Working Group I to the Fourth Assessment Report of the Intergovernmental Panel on Climate Change. Cambridge University Press, Cambridge, pp. 747–845.

Moreno-de las Heras, M., Merino-Martín, L., Nicolau, J.M., 2009. Effect of vegetation cover on the hydrology of reclaimed mining soils under Mediterranean-Continental climate. Catena 77, 39–47.

Müller, K., Deurer, M., Jeyakumar, P., Mason, K., van den Dijssel, C., Green, S., Clothier, B., 2014. Temporal dynamics of soil water repellency and its impact on pasture productivity. Agric. Water Manag. 143, 82–92.

Müller, K., Mason, K., Gastelum, Strozzi A., Simpson, R., Komatsu, T., Kawamoto, K., Clothier, B., 2018. Runoff and nutrient loss from a water-repellent soil. Geoderma 322, 28–37.

Nyman, P., Sheridan, G., Lane, P.N.J., 2010. Synergistic effects of water repellency and macropore flow on the hydraulic conductivity of a burned forest soil, south-east Australia. Hydrol. Process. 24 (20), 2871–2887.

Orfánus, T., Dlapa, P., Fodor, N., Rajkai, K., Sándor, R., Nováková, K., 2014. How severe and subcritical water repellency determines the seasonal infiltration in natural and cultivated sandy soils. Soil Tillage Res. 135, 49–59.
Orfánus, T., Stojkovová, D., Rajkai, K., Czachor, H., Sándor, R., 2016. Spatial patterns of wetting characteristics in grassland sandy soil. J. Hydrol. Hydromech. 64, 167–175.
Pekárová, P., Pekár, J., Lichner, L., 2015. A new method for estimating soil water repellency index. Biologia 70, 1450–1455.
R Core Team, 2016. Language and Environment for Statistical Computing. R Foundation for Statistical Computing, Vienna, Austria http://www.R-project.org.
Rillig, M.C., Mardatin, N.F., Leifheit, E.F., Antunes, P.M., 2010. Mycelium of arbuscular mycorrhizal fungi increases soil water repellency and is sufficient to maintain water-stable soil aggregates. Soil Biol. Biochem. 42, 1189–1191.
Robinson, D.A., Lebron, I., Ryel, R.J., Jones, S.B., 2010. Soil Water Repellency: A Method of Soil Moisture Sequestration in Pinyon–Juniper Woodland. Soil Sci. Soc. Am. J. 74, 624–634.
Rodríguez-Alleres, M., Benito, E., 2011. Spatial and temporal variability of surface water repellency in sandy loam soils of NW Spain under *Pinus pinaster* and *Eucalyptus globulus* plantations. Hydrol. Process. 25, 3649–3658.
Roper, M.M., 2005. Managing soils to enhance the potential for bioremediation of water repellency. Aust. J. Soil Res. 43, 803–810.
Roper, M.M., 2006. Potential for remediation of water repellent soils by inoculation with wax-degrading bacteria in southwestern Australia. Biologia 61 (Suppl. 19), S358–S362.
Rye, C.F., Smettem, K.R.J., 2017. The effect of water repellent soil surface layers on preferential flow and bare soil evaporation. Geoderma 289, 142–149.
Sándor, R., Lichner, L., Filep, T., Balog, K., Lehoczky, É., Fodor, N., 2015. Spatial variability of hydrophysical properties of fallow sandy soils. Biologia 70, 1468–1473.
Sepehrnia, N., Hajabbasi, M.A., Afyuni, M., Lichner, L., 2016. Extent and persistence of water repellency in two Iranian soils. Biologia 71, 1137–1143.
Sepehrnia, N., Bachmann, J., Hajabbasi, M.A., Rezanezhad, F., Lichner, L., Hallett, P.D., Coyne, M., 2019. Transport, retention, and release of *Escherichia coli* and *Rhodococcus erythropolis* through dry natural soils as affected by water repellency. Sci. Total Environ. 694, 1–8.
Staff, Soil Survey Division, 1993. Soil Survey Manual. Soil Conservation Service. U.S, Department of Agriculture Handbook, p. 18.
Täumer, K., Stoffregen, H., Wessolek, G., 2005. Determination of repellency distribution using soil organic matter and water content. Geoderma 125, 107–115.
Täumer, K., Stoffregen, H., Wessolek, G., 2006. Seasonal dynamics of preferential flow in a water repellent soil. Vadose Zone J. 5, 405–411.
Walsh, P.D., Lawler, D.N., 1981. Rainfall seasonality: description, spatial patterns and change through time. Weather 36, 201–208.
Ward, P.R., Roper, M.M., Jongepier, R., Micin, S.F., 2015. Impact of crop residue retention and tillage on water infiltration into a water-repellent soil. Biologia 70, 1480–1484.
WRB, 2014. World Reference Base for Soil Resources 2014. World Soil Resources Reports No. 106. Rome, 192 p.
Zhang, R., 1997. Determination of soil sorptivity and hydraulic conductivity from the disk infiltrometer. Soil Sci. Soc. Am. J. 61, 1024–1030.